



LAWRENCE
LIVERMORE
NATIONAL
LABORATORY

A Validation of FEM3MP with Joint Urban 2003 Data

S. T. Chan, M. J. Leach

August 29, 2006

Journal of Applied Meteorology

Disclaimer

This document was prepared as an account of work sponsored by an agency of the United States Government. Neither the United States Government nor the University of California nor any of their employees, makes any warranty, express or implied, or assumes any legal liability or responsibility for the accuracy, completeness, or usefulness of any information, apparatus, product, or process disclosed, or represents that its use would not infringe privately owned rights. Reference herein to any specific commercial product, process, or service by trade name, trademark, manufacturer, or otherwise, does not necessarily constitute or imply its endorsement, recommendation, or favoring by the United States Government or the University of California. The views and opinions of authors expressed herein do not necessarily state or reflect those of the United States Government or the University of California, and shall not be used for advertising or product endorsement purposes.

A Validation of FEM3MP with Joint Urban 2003 Data

Stevens T. Chan* and Martin J. Leach

Lawrence Livermore National Laboratory, Livermore, California 94551, USA

* *Corresponding author address:* S. T. Chan, Lawrence Livermore National Laboratory, P.O. Box 808, L-103, Livermore, CA 94551, Phone: (925) 422-1822, Fax: (925) 422-5844, E-mail: schan@llnl.gov

Abstract

Under the sponsorship of the U.S. DOE and DHS, we have recently developed a computational fluid dynamics (CFD) model for simulating airflow and dispersion of chemical/biological agents released in urban areas. Our model, FEM3MP, is based on solving the three-dimensional, time-dependent Navier-Stokes equations with appropriate physics submodels on massively parallel computer platforms. It employs finite-element discretization for effective treatment of complex geometries and a semi-implicit projection scheme for efficient time-integration. A simplified CFD approach, using both explicitly resolved and virtual buildings, was implemented to further improve the model's efficiency. Predictions from our model are continuously being verified against measured data from wind tunnel and field studies. Herein our model is further evaluated using observed data from IOPs (intensive operation periods) 3 and 9 of the Joint Urban 2003 field study conducted in Oklahoma City, Oklahoma, in July 2003. Our model predictions of wind and concentration fields in the near and intermediate regions, as well as profiles of wind speed, wind direction, friction velocity, and turbulent kinetic energy (TKE) in the urban wake region, are generally consistent with and compared reasonably well with field observations. In addition, our model was able to predict the observed split plume of IOP 3 and the end vortices along Park Avenue in IOP 9. The dispersion results and TKE profiles at the crane station indicate the effects of convective mixing are relatively important for the daytime release of IOP 3 but the stable effects are relatively unimportant for the nighttime release of IOP 9. Results of this study also suggest that the simplified CFD approach implemented in FEM3MP can be a cost-effective tool for simulating urban dispersion problems.

1. Introduction

Urban areas are the mostly likely locations for atmospheric releases of hazardous material, whether due to industrial accidents or terrorist acts. In order to protect the population effectively, there is a great need for observational and modeling tools to track and forecast the transport and dispersion of the hazardous material from such releases. The need for robust modeling tools, among others, was stressed in a recent report by the National Research Council of the National Academies (2003). Amongst the recommended priorities for improving modeling capabilities, the report states ‘New dispersion modeling constructs need to be further explored and possibly adapted for operational use in urban settings. This includes advanced, short execution time models, slower but more accurate computational fluid dynamics and large-eddy simulation models, and models with adaptive grids’.

Under the sponsorship of the U.S. Department of Energy (DOE) and Department of Homeland Security (DHS), we have recently developed a computational fluid dynamics (CFD) model for simulating airflow and dispersion of chemical/biological agents released in the urban environment. Our model, FEM3MP, is based on solving the three-dimensional, time-dependent, incompressible Navier-Stokes equations on massively parallel computer platforms. The numerical algorithm is based on finite-element discretization for effective treatment of complex building geometries and variable terrain, together with a semi-implicit projection scheme and modern iterative solvers developed by Gresho and Chan (1998) for efficient time-integration. Physical processes treated in our code include turbulence modeling via the Reynolds Averaged Navier-Stokes (RANS) and Large Eddy Simulation (LES) approaches (Chan and Stevens, 2000), aerosols (Chan et al., 1999), UV radiation decay, surface energy budgets (Lee and Brown, 2001), and vegetative canopies (Chan et al., 2002).

Predictions from our model are continuously being verified against measured data from wind tunnel and field studies. Some of the model evaluation studies using wind tunnel data were reported in Chan and Stevens (2000) and Chan et al. (2001). Examples of model evaluations using observed data from various field experiments were documented in Calhoun et al. (2004, 2005), Chan et al. (2003), Lee et al. (2002), and Humphreys et al. (2003).

Besides model evaluation studies, our model has also been used to investigate the effects of inflow turbulence on dispersion scenarios involving nighttime releases under light and highly variable winds, such as the case of IOP 7 of the URBAN 2000 experiment (Allwine et al., 2002). Through a series of controlled numerical experiments with various time-dependent forcing and turbulence intensity from the inflow boundary, Chan and Leach (2004) demonstrated that, in order to successfully simulate urban dispersion scenarios under light and highly variable winds, it is necessary to use appropriate time-dependent forcing and turbulence from the larger scale flow through the inflow boundary. Their results also indicate that inflow turbulence is as important, if not more so, than building-induced mechanical turbulence in dispersion scenarios under the above conditions.

While high-resolution CFD models are very useful for emergency planning, vulnerability analyses and post-event analyses, such models usually require excessive computer resources and long turnaround times, thus rendering them unsuitable for emergency response applications. Our goal is to develop a sufficiently fast CFD urban dispersion model for integration into the DOE National Atmospheric Release Advisory Center (NARAC) operational modeling system. As a step toward reaching such a goal, a simplified CFD approach, with options to use either virtual buildings (represented as larger drag forces) only or a combination of explicitly resolved and virtual buildings, has been developed (Chan et al., 2004). With the later option, only targeted and

important buildings are explicitly resolved using fine grid resolution and the remaining buildings are modeled as virtual buildings using coarser grid resolution. The drag forces were modeled as a sink term in the mean momentum equations, similar to the canopy-drag term proposed by Yamada (1982) and Brown and Williams (1998).

In this paper, the FEM3MP model is further evaluated in a more detailed comparison against a subset of the data collected in the Joint Urban 2003 field study. Specifically, our model using both explicitly resolved and virtual buildings was used to simulate the first continuous release of intensive operation periods (IOPs) 3 and 9, and predicted results of wind and concentration in the near and intermediate regions (from the source locations), as well as profiles of wind speed, wind direction, friction velocity, and TKE at the pseudo-tower location in the urban wake region, are compared against the field observations. In the following, we first give a brief description of the simplified CFD approach implemented in FEM3MP, then discuss briefly the field experiments being simulated, present a comparison between model predictions and observed data, and finally offer a few concluding remarks.

2. A simplified CFD approach

For convenience of code parallelization and computational speed, our current version of FEM3MP employs a structured mesh (but graded and distorted mesh is allowed) and buildings within the computational domain are represented as solid blocks with velocity, pressure, and diffusivities set equal to 0. The crux of our simplified CFD approach (Chan et al., 2004) is to explicitly resolve targeted and important buildings with fine grid resolution and to treat the remaining buildings as virtual buildings with coarser grid resolution. An initial evaluation of the

approach, using data from the Joint Urban 2003 field experiment (Allwine et al., 2004), can be found in Humphreys et al (2004).

The virtual buildings are modeled as drag forces in the mean momentum equations via a term similar (but not identical) to the canopy-drag term proposed by Yamada (1982) and Brown and Williams (1998). More specifically, at grid points associated with the virtual buildings, a term in the form of $C_d |U| U_i$, where C_d is a drag coefficient (of unit 1/m), $|U|$ is the local wind speed, and U_i is the i^{th} velocity component, is added to the mean momentum equations. By using a large value of the drag coefficient, as will be seen in the example below, a virtual building can be made to act like an explicitly resolved (solid) building. The drag term is linearized and treated implicitly in the time stepping algorithm. In addition, the diffusivities at the corresponding grid points are set equal to the molecular diffusivity of air, instead of zero, in order to avoid numerical instability.

Besides computational efficiency, the virtual building approach also offers the advantages of much easier grid generation and a direct means for evaluating the drag forces to aid the parameterization of urban canopy in larger scale CFD models. However, predicted results in the vicinity of the virtual buildings are, as expected, slightly less accurate, because coarser grids are used and small values of velocity and diffusivities (instead of zero) are present as a result of the drag force approximation.

The following simple example, using a relatively coarse grid, shows how the virtual building approach performs in simulating the airflow and tracer dispersion around a cubical building of unit dimension ($H=1$). Four simulations were performed. The cubical building was explicitly resolved (as a solid building) in one simulation and modeled as a virtual building (drag forces) with a drag coefficient of 15, 50, and 100 respectively in the remaining simulations. A

computational domain of $8H \times 6H \times 2H$ in the longitudinal, lateral, and vertical directions, with a graded mesh consisting of $43 \times 33 \times 15$ grid points was used in all simulations. For simplicity, a logarithmic velocity profile, with $u_* = 0.0356$ m/s, $z_0 = 0.001$ m, and $U = 0.6$ m/s at H , was specified on the inlet plane and a similarity K-theory model (Dyer, 1974) was used for turbulence parameterization. In each case, a steady state wind field was established first (after 60 sec simulated time) and then followed by the dispersion simulation associated with a ground level tracer released continuously over an area of 2 cells at $1.5H$ in front of the cube for a duration of 120 sec.

In Fig. 1, the predicted steady-state velocity and normalized concentration on the vertical plane of symmetry with the cube modeled as a virtual building (top three panels) and as a solid building (bottom panel) are shown. The normalized concentration is defined as $X = C \cdot U \cdot H^2 / Q$, in which C is the calculated concentration (mass fraction), U is the reference velocity at H , and Q is the source rate. Predicted wind vectors obtained from the virtual-building simulations indicate that, as the drag coefficient is increased to 100, the wind speeds and airflow patterns, including flow separation on the rooftop, a small eddy and the indication of a dividing streamline on the windward side and a large eddy on the leeward side of the cubical building, become very close to those obtained from the simulation using the solid-building approach. A similar trend of convergence is observed for the concentration field.

In Fig. 2, the corresponding velocity vectors and concentration field on the plane $z/H = 0.2$ obtained from the four simulations are compared. Again, as the drag coefficient is increased to 100, results from the virtual-building approach become very close to those obtained from the run using the solid-building approach. The similar features include a diverging flow in the front, separation on the sides, and a reverse flow with two counter-rotating vortices in the wake region,

as well as the horseshoe-shaped concentration patterns on the plane. These results suggest that a drag coefficient of $O(100)$ is a reasonable parameter to use.

As alluded to earlier, due to the approximate nature of the predicted flow in the vicinity of the virtual building, less accurate predictions, such as spurious infiltration of the tracer (of lower concentrations) into the virtual building, are expected. It must be emphasized that the main idea of the simplified CFD approach is to use virtual buildings judiciously in places where large gradients of the concentration field are absent and also at locations where only reasonably accurate results are warranted. In these respects, the present example is a severe test of the virtual building approach and the present results are considered reasonable. Explicitly resolved buildings should always be used wherever highly accurate predictions are important.

Using four 2.4 GHz Xeon processors, the CPU times required to generate the steady-state flow field by the runs using the virtual-building approach (with $C_d = 15, 50, 100$) are 131, 133, and 134 sec, respectively, while the solid-building approach requires 136 sec. Total CPU times required for the four dispersion simulations are basically the same. The savings in computational cost by using the virtual-building approach, although insignificant, are nevertheless noticeable. For practical urban dispersion simulations, which involve typically hundreds or more buildings, the savings in computational cost by modeling a large fraction of the buildings as virtual buildings can be significant. For instance, in simulating a hypothetical tracer gas release in the Salt Lake City downtown area involving $O(100)$ buildings with an all virtual-building approach, together with a coarser grid (than the one used in an all solid-building approach), Chan et al. (2004) were able to reproduce reasonably well the main features of concentration patterns predicted by the all solid-building approach, but with an order-of-magnitude savings in computational cost.

The option of using only virtual buildings has been developed with certain category of emergency response applications in mind, for which airflow in street canyons still needs to be fairly well resolved but a compromise between accuracy and computational speed is definitely required. This type of applications may become feasible with a simplified CFD approach using only virtual buildings, together with a simple turbulence model, a relatively coarse and graded grid, and modest computer resources. For these reasons, the value of drag coefficient was made based on a simple K-theory turbulence model. The value of drag coefficient should perhaps have been calibrated for the NEV turbulence model as well; however, computational time could increase greatly due to the necessity of solving three additional (turbulence) equations and the need of finer grid resolution in order to fully realize the higher accuracy offered by the NEV turbulence model. Therefore the combination of virtual buildings and NEV turbulence model has not been considered for emergency response applications. Nevertheless, some of our recent urban dispersion simulations have been made using virtual buildings exclusively, together with either LEV or NEV turbulence models. Results from these simulations seem to indicate the same value of drag coefficient is appropriate for both turbulence models.

3. The Joint Urban 2003 field study

In order to provide quality-assured, high-resolution meteorological and tracer data sets for evaluation and validation of indoor and outdoor urban dispersion models, the U.S. DHS and DoD – Defense Threat Reduction Agency (DTRA) co-sponsored a series of dispersion experiments, named Joint Urban 2003 (JU2003), in Oklahoma City (OKC), Oklahoma, during July 2003 (Allwine et al., 2004). These experiments are complementary to the URBAN 2000 field study (Allwine et al., 2002) in that they provide another comprehensive field data set for the

evaluation of CFD and other dispersion models. In contrast to the URBAN 2000 experiments, which were conducted entirely at night, these experiments took place during daytime and nighttime to include both convective and stable atmospheric conditions. Prior to the field study, FEM3MP simulations were performed to provide guidance for the selection of release sites and the deployment of wind and concentration sensors.

A total of ten IOPs were conducted and SF₆ in the form of puffs or continuous sources were released over 6 daytime and 4 nighttime episodes. Many wind and concentration sensors were used to collect wind and SF₆ data over both long and short time-averaging periods. In addition to surface measurements, wind and concentration profiles adjacent to the outside walls of several buildings were also taken. In some cases, balloons were deployed close to the tracer release area. Many of the released balloons exhibited quick ascents from ground level to the rooftop of buildings, implying highly convective conditions.

During the JU2003 experiment, a pseudo-tower, supported by a 90-m crane and fitted with sonic anemometers at eight levels, was also deployed for wind and turbulence observations. The pseudo-tower (crane station) was located in the urban wake region at approximately 750 m NNW from the OKC central business district. Winds, temperature, and turbulence data collected on the pseudo-tower have been analyzed by Lundquist and Chan (2005) to construct profiles of wind speed, wind direction, friction velocity, and TKE. These observed profiles are also used in this model evaluation study.

All of the data used in this study were downloaded from the JU2003 website (<https://ju2003-dpg.dpg.army.mil>). The locations used were those reported in the README files, or in the file metadata. All data locations that were reported in latitude-longitude were converted to UTM coordinates using standard conversion algorithms. The wind data was averaged to 30 minutes

from the various sensors, either by averaging the original 10Hz data, or by averaging data that had previously been averaged over shorter time intervals. The tracer data used for comparison to model predictions had been obtained by using 15-minute or 30-minute averaging time.

4. Modal-data comparison

In this study, airflow and dispersion simulations associated with the first continuous release of IOPs 3 and 9, which are daytime and nighttime releases respectively, were performed. In each case, SF₆ was released near the ground as a point source for 30-min, with a release rate of 5.0 g/s for IOP 3 and 2.0 g/s for IOP 9. Shown in Fig. 3 are the footprints of buildings in the central business district of OKC, with the release locations indicated by S3 for IOP 3 and S9 for IOP 9. The tallest building in the area is approximately 120-m high and the average building height in the area is ~30 m.

In the numerical simulations, a computational domain of 1,030 m x 3,010 m x 425 m (in the lateral, longitudinal, and vertical directions) was used. A graded mesh consisting of 201 x 303 x 45 grid points, with a minimal grid spacing of ~1 m near the ground surface and certain explicitly resolved buildings, was used. Most of the buildings within ~500 m of the release points were explicitly resolved and the remaining buildings were modeled as virtual buildings.

Steady logarithmic velocity profiles were constructed from nearby sodar and weather station observations and used as the inflow conditions. The resulting wind speed at $z=50$ m is 6.5 m/s for IOP 3 and 7.2 m/s for IOP 9; the estimated average wind direction is 185° for IOP 3 and 180° for IOP 9. A comparison of the inflow wind speed and direction profiles (solid lines) against sodar data (dashed lines) for the two IOPs is shown in Fig. 4, indicating the constructed

profiles are a reasonable representation of the observations. Based on the sodar and sonic anemometer data we examined, directional shear and vertical motion do not appear to be significant for the simulated releases. However, for IOP 8, due to the presence of a nocturnal low-level jet (Lundquist and Mirocha, 2006), directional shear and vertical motion may be significant and may have to be considered in numerical simulations.

FEM3MP does have the capability to use a realistic profile (including wind shear and time variations) other than a logarithmic profile. However, appropriate measurements for defining detailed inflow profiles are not available, thus logarithmic profiles were constructed from nearby sodar and weather observations and used in our simulations. Since the stable nocturnal conditions exhibited by the observed surface data in Fig. 4 do not appear to be representative of the nearly neutral atmospheric conditions observed elsewhere and are thus not incorporated into the inflow conditions. However, our model predictions (to be shown later) for winds and concentration field in OKC downtown and urban wake regions are generally consistent with observations, which seem to suggest that flow and concentration in the downtown and wake regions are only weakly affected by upwind surface winds (below the average building height). This is probably true, because winds below the average building height are often greatly altered by buildings in the urban area, in addition to the changes caused by the upwind fetch (which is about 600 m long in our domain of simulations). In general, appropriate inlet boundary conditions are important for accurate flow and dispersion simulations and should be further studied in the future.

For IOP 3 (Fig. 4a), the actual wind and direction profiles are from a sodar deployed in the botanical gardens about 100 meters to the south of the release point. For IOP 9 (Fig. 4b), the observed wind speed and direction profiles are from a sodar about 4 km downwind of OKC. We

recognize that this is downwind, but feel that it is more representative of the upwind conditions of the release, for which the crane data (to be shown later) indicate the atmospheric conditions for this nighttime release were nearly neutral. The sodar observations from the botanical gardens and another upwind site at the Oklahoma City maintenance yard exhibited characteristics of a nocturnal decoupling of the surface layer from the boundary layer above. Such stable nocturnal conditions do not appear to be representative of the nearly neutral atmospheric conditions observed elsewhere.

On the inflow boundary, the above velocity profile, together with values of tke and ϵ (of the turbulence equations) consistent with the specified velocity profile, was imposed. On the walls of the explicitly resolved buildings and ground surface, no-slip boundary conditions (zero velocity) and zero values of tke and ϵ were specified. No penetration (zero vertical velocity) was applied on the top boundary and natural boundary conditions (zero normal and tangential stresses) were used on the remaining boundary.

For each simulated release, a quasi-steady state flow field was first established after ~ 10 minutes of simulated time before the tracer was released. The release of SF_6 was modeled as a continuous source over a small area (covered by 2×2 cells on the ground surface) at a constant release rate and dispersion results indicate steady state was reached in about 20 minutes of simulated time. For both cases, the RANS approach with a non-linear eddy viscosity (NEV) turbulence model (Gresho and Chan, 1998) was used and neutral atmospheric stability was assumed.

In the following, model predictions of flow and concentration in the near and intermediate regions of the release point are presented and compared with observed data. Several of the statistical performance measures recommended by Hanna et al. (2005) are used to assess the

performance of our model. They are: the fraction of predictions within a factor of two or five (FAC2 or FAC5), fractional bias (FB), geometric mean bias (MG), and normalized mean square error (NMSE). For differences in angles between predicted and measured velocity vectors, the formula of scaled average angle differences (SAA) devised by Calhoun et al. (2004), with larger vectors carrying more weights, is also used.

The equations for these metrics are defined as:

$$\begin{aligned}
 FB &= \frac{(\overline{C_o} - \overline{C_p})}{0.5(\overline{C_o} + \overline{C_p})}, \\
 MG &= \exp \left[\ln \left(\frac{\overline{C_o}}{\overline{C_p}} \right) \right], \\
 NMSE &= \frac{(\overline{C_o} - \overline{C_p})^2}{\overline{C_o} \overline{C_p}},
 \end{aligned}$$

and

$$FACx = \text{fraction of data for which } \frac{1}{x} \leq \frac{C_p}{C_o} \leq x,$$

in which C is the data being evaluated (e.g., wind speed or tracer concentration), C_p is the model prediction, and C_o is the observation, with overbars denoting averages. In the above metrics, FB and MG measure the systematic bias of a model in terms of differences and ratios, and NMSE measures the scatter associated with the predictions relative to observations. A perfect model would have $FACx = 1.0$, $FB = 0$, $MG = 1.0$, and $NMSE = 0$.

The SAA, a model performance metric calculated from wind speeds and wind directions, is given by

$$SAA = \frac{(\sum |U_i| |\phi_i|)}{(N |\overline{U_i}|)},$$

in which ϕ_i is the angle between predicted and observed velocity vectors and N is the number of samples being averaged. The angle difference is scaled by the magnitude of the predicted velocity vector $|U_i|$ and then is normalized by the average of the magnitudes over all samples. By scaling the angles by the magnitudes, this metric weights the angles of the larger vectors more strongly to minimize the relatively unimportant errors in wind direction associated with small wind speeds.

Additionally predicted and observed profiles of wind speed, wind direction, friction velocity, and turbulent kinetic energy (TKE) at the crane station (at about 750 m NNW from the OKC central business district) are compared. The friction velocity u_* is calculated by assuming that the profile of wind speeds fit the relationship

$$u_* = \frac{kU}{\ln(z/z_o)},$$

in which k is the von Karman constant of 0.4, U is the mean wind speed at each height z , and surface roughness z_o is set to 0.5 m in the urban wake.

4.1 IOP 3

Airflow in urban areas is extremely complex, as is illustrated in Fig. 5 for IOP 3. In the figure, predicted wind vectors and corresponding wind speeds (gray scale contours) near the ground ($z=2$ m) are displayed. Some of the complex flow features include flow separations, stagnation zones, various sizes of eddies, and high velocity jets in street canyons. Also, it is interesting to see how the flow separates at the SW corner of the building in the center, which is obviously the cause of a split plume as will be shown later.

In Fig. 6, the predicted wind vectors (without arrow heads) in the downtown area are compared with the 30-min averaged data (with arrow heads) measured by Dugway Proving

Ground (DPG) PWIDS and sonic anemometers on three towers along Park Avenue ($y=430$ to 460 m). Overall, the agreement between model predictions and field observations is good. The values of statistical performance measures are: $SAA=25.3$, $FAC2=0.74$, $FB=-0.21$, $MG=0.79$, and $NMSE=0.30$, respectively.

There were several anemometers at various levels on each of the towers along Park Avenue. Only the level from the tower nearest to 8 meters is used to compare to the simulations from FEM3MP. For this IOP, there is reasonably good agreement, especially for the two westernmost towers. For the tower near the eastern end of the Park Avenue, the observed wind vector is much smaller in magnitude with close to a 90-degree direction error. This tower was near a bank of trees that was not represented in the FEM3MP simulations and this smaller vector may represent vegetation canopy effects.

In Fig. 7, a comparison of predicted versus observed profiles of wind speed, wind direction, friction velocity, and TKE is presented. In general, there is a reasonable agreement between the predicted and observed profiles for wind speed and friction velocity, with the predicted values in the range of 60-75% of the observations. The wind direction profiles indicate that the simulated wind direction is likely off by 5-15 degrees. In the lower right panel, profiles of simulated, observed, and observed minus buoyant TKE are presented. The shapes of the TKE profiles are fairly similar, with the predicted TKE values in the range of 50-90% of the observed values. As is seen in the panel, the estimated buoyant contribution to the total observed TKE is only 10% at maximum.

A discussion of the TKE budget and evaluation of TKE and its dissipation rate from the crane data can be found in Lundquist and Chan (2005). To estimate the contribution of buoyant forcing to the total TKE, the rate of buoyant production is multiplied by a turbulent time scale τ ,

which is determined from the quotient of TKE over the dissipation rate, following the model of Zeierman and Wolfshtein (1986). The estimated turbulent time scales for the two simulated experiments are 40-145 sec for IOP 3 (a daytime release) and 70-85 sec for IOP 9 (a nighttime release) respectively.

The predicted concentrations (solid line) along Broadway Avenue (at abscissa $x=115$ to 150 m in Fig. 6) are compared against the time-averaged data (circles) in Fig. 8. The model predictions are from $x=140$ m and the field data is a collection of observations from sensors located near $x=140$ m, with most of the data averaged over $t=15$ to 30 min. The exceptions are values at downwind $y=670$ m, 775 m, and 890 m, which were averaged over $t=0$ to 30 min. The agreement is good and within a factor of two in the urban area (downwind distance $y<600$ m), beyond which the predicted values are much higher than observed. The discrepancies are mainly attributable to the following: the observed values at $y=670$ m, 775 m, and 890 are most likely too low because they were obtained with a 30-min averaging time (for a 30-min release), the gas sensors might have been too far apart (~ 200 m at the 2000-m arc) to capture the higher concentration values, and the assumption of neutral atmospheric conditions in our current NEV turbulence model may not be appropriate in the urban wake region and beyond. In order to evaluate the stability effects, another simulation using a linear eddy viscosity (LEV) turbulence model based on the similarity K-theory (Dyer, 1974), together with an estimated Monin-Obukhov length of -200 m, was performed. A better agreement between model predictions (dashed line) and data in the far field was indeed observed. However, the agreement in the near field is not as good due to a less sophisticated representation of turbulence near buildings.

The LEV model is actually a simplified version, i.e., without heavy gas effects, of the modified K-theory turbulence model developed by Chan et al. (1987) for simulating atmospheric

dispersion of heavy gases over variable terrain. The model accounts for turbulence due to atmospheric stability but no explicit treatment for building-induced turbulence. Thus the model is more appropriate for upwind and regions further away from the urban area. Despite its simplicity and being less accurate than other turbulence models such as NEV and LES, the LEV turbulence model is capable of capturing the major features of airflow around a complex building (Calhoun et al., 2004) and has also been observed to perform reasonably well in one of our recent urban flow and dispersion studies (Lundquist and Chan, 2005). On the other hand, the NEV model (Gresho and Chan, 1998) has treated building-induced turbulence explicitly through solving three additional equations for turbulence and is more appropriate for urban flow and dispersion simulations in general. However, our present version of NEV model can treat only airflow under nearly neutral atmospheric conditions. Without including the stability effects, results can be inaccurate in regions where atmospheric stability plays an important role, such as the urban wake and further downwind regions.

In Fig. 9, predicted concentration patterns in the source area are compared against the measured data (small squares with the same color scheme). Except for missing or under-predicting a few very low concentrations near the left edge of the plume, the predicted concentrations generally agree well with the observations. In addition, the simulation was able to predict a split plume in front of the building nearby. The values of statistical performance measures are: $FAC5=0.42$, $FB=-0.56$, $MG=6.2$, and $NMSE=14$. The values of MG and $NMSE$ are high due to a bias produced by the presence of two high concentrations (one is near the edge of the plume and the other is to the south of the building) within a small sampling population. Hanna et al. (2005) pointed out that the values of MG and $NMSE$ could be overly influenced by infrequently occurring high observed and/or predicted data. When the two pairs of highest

concentrations were excluded in the performance evaluation, the values of statistical performance measures became: $FAC5=0.50$, $FB=-0.35$, $MG=4.82$, and $NMSE=0.61$, respectively.

4.2 IOP 9

In this subsection, sample flow and dispersion results from simulations of the IOP 9 release are presented and compared with available data. In Fig. 10, the predicted wind vectors and speeds (gray scale contours) in the source area are depicted to illustrate again the complexity of airflow in an urban area, including stagnation zones in front of the buildings, flow separations on the sides, jetting in street canyons, and large wakes behind buildings. In addition, there are two counter-rotating vortices behind the wide building on the south side of Park Avenue ($y=430-460$ m). Such end vortices were also reported by Brown et al. (2004) in the field study. Another interesting feature of the wind field is the strong reverse flow (northerly winds within the NW quadrant of the picture) in front of the 105-m tall Kerr McGee building (near the north edge of the picture).

In Fig. 11, predicted wind vectors in the downtown area are compared with the 30-min averaged data measured by DPG PWIDS and sonic anemometers on four towers along Park Avenue ($y=430$ to 460 m). Again, the overall agreement between model predictions and field measurements is good, especially in the source area (middle of picture). The statistical performance measures are similar to the previous case: $SAA=34.2$, $FAC2=0.71$, $FB=-0.20$, $MG=0.98$, and $NMSE=0.48$.

In this IOP, the observed winds along Park Avenue are more variable. Again, only the wind vectors from the towers nearest the 8-m level along Park Avenue are compared. The vectors

agree very well at the more southern tower in mid-block and at the westernmost tower, where both the simulation and observation show very light wind speeds. The wind vectors do not agree well at the more northern mid-block tower or at the tower near the east end of Park Avenue. The observations hint at the existence of a counter-clockwise eddy in the eastern half of the block, while the simulation has such an eddy but it does not penetrate as far west in the urban canyon (see Fig. 10). Some of the discrepancies may be due to the use of the 180° wind direction for the inflow conditions.

A close comparison between Figs. 6 and 11 reveals that some of the wind vectors are significantly different in speed and direction, even though the inflow wind directions differ merely by 5° and the wind speeds differ only by $\sim 10\%$.

In Fig. 12, the predicted versus observed profiles of wind speed, wind direction, friction velocity, and TKE are compared. In general, the shapes of the predicted profiles are in good agreement with those observed. The wind speeds are slightly over-predicted compared to observations, while the wind direction is about 10 to 15 degrees away from observed wind directions. Predicted values of friction velocity are slightly greater than observed, which is consistent with the slightly over-predicted wind speeds. The TKE profiles predicted by the model agree quite well with those observed at the crane location and the role of buoyancy is minimal during this nocturnal release. Again, the contribution of buoyant forcing to the total TKE was obtained by the product of the rate of buoyant production multiplied by a turbulent time scale τ , which is determined from the quotient of TKE over the dissipation rate, following the model of Zeierman and Wolfshtein (1986). The estimated turbulent time scale for this nighttime release is 70-85 sec.

Due to the southerly ambient winds and a lower source rate (2.0 g/s instead of 5.0 g/s) released in the middle of Park Avenue, observed concentrations along Broadway Avenue were much lower than those observed in IOP 3. In addition, some of the data were not usable because of missing samples, field sampling problems, or problems during laboratory analysis. For these reasons, it was decided to compare the downwind concentration along the plume ‘centerline’ instead.

In Fig. 13, predicted concentrations (solid line) along the plume ‘centerline’ (at abscissa $x=32$ m in Fig. 11) are compared against the time-averaged data (circles). The field data is a collection of observations from sensors located near $x=32$ m, with most of the data averaged over $t=15$ to 30 min. Two exceptions are the values at downwind $y=775$ m and 2370 m, which were averaged over $t=0$ to 30 min. Despite considerable under-predictions in the near field (downwind distance $y<800$ m), the overall agreement between model predictions and observations is within a factor of two. In order to evaluate the stability effects, a simulation using the LEV turbulence model based on the similarity K-theory (Dyer, 1974), together with an estimated Monin-Obukhov length of 300 m, was performed. In this case, the simulation using the LEV model, together with parameterization for stable stratification, was unable to yield the higher concentrations expected for all locations, because the LEV model is not sophisticated enough to model the complexity of turbulence near buildings and in the wake region.

Unlike the daytime release of IOP 3, dispersion results in the intermediate region and beyond are only slightly affected by the slightly stable atmospheric stability. These results are consistent with the observed TKE data at the crane station (lower right panel of Fig. 12), which indicates any turbulence reduction due to the slightly stable conditions at night is minimal. Considering this fact and the finding by Lundquist and Chan (2005) that building-induced

turbulence is dominant in an urban area, it is justifiable to use the neutral stability assumption for this nighttime dispersion simulation.

The predicted concentrations in the source area are compared against measured data in Fig. 14. Again, except for a few locations near the western edge of the plume, the predicted results generally agree well with the observed data. In addition, the model was able to predict the unusually high concentration of over 500 ppb near the east end and south side of Park Avenue. The counter-clockwise vortex near the east end of the street is believed to be mainly responsible for producing such a surprisingly high concentration at the location. As quantitative measures of model performance, the statistical performance measures are: $FAC5=0.56$, $FB=-0.39$, $MG=2.0$, and $NMSE=0.96$, respectively.

As mentioned earlier, balloons released as visible tracers during some of the experiments exhibited quick ascents from ground level to the top of buildings, implying significant updrafts during those experiments. In Fig. 15, updrafts in street canyons and their effects on tracer dispersion are illustrated. In Fig. 15(a), the predicted and observed concentration profiles on the outside walls of the building (B1) at the northeast corner of Park Avenue in Fig. 14 are compared. In general, our model predictions are able to reproduce a lofting plume observed in the field and also match fairly well with the measured values, mostly within a factor of 3. The largest over-predictions occur at the south and east sides of B1, which are very likely due to the inaccurate inflow direction used in the simulation. The estimated inflow direction may be off by 10 to 15 degrees, as suggested by results in the upper right panel of Fig. 12. Since there is a large open space with some lower buildings on the south and east sides of B1, specifying an inflow direction of 165-170 (rather than 180) degrees would have resulted in more airflow to reduce the predicted concentrations on those sides of the building to make the predictions agree better with

the observed data. In Fig. 15(b), the predicted concentrations and wind vectors on the plane cutting through the source ($x=32$ m) is shown. The wind vectors show clearly the strong updrafts in building wakes and intense vortex motions around the buildings. As a result, the plume rises and reaches above the rooftops of certain buildings.

5. Conclusions

In this paper, FEM3MP has been evaluated using wind and concentration data obtained from IOPs 3 and 9 of the Joint Urban 2003 experiment. Our model predictions for the two IOPs, regarding both wind and concentration fields in the near and intermediate regions, as well as profiles of wind speed, wind direction, friction velocity and TKE at the crane station, are generally consistent with and compared reasonably well with field observations. In addition, our model was able to predict the split plume observed in IOP 3 and the end vortices and an unusually high concentration near the east end of Park Avenue observed in IOP 9.

Judging from the crane data and predicted dispersion results, the effects of convective mixing in the daytime release (IOP 3) appear to be relatively important in the intermediate (urban wake) region and should be considered appropriately. On the other hand, for the nighttime release of IOP 9, the crane data indicate any turbulence reduction due to the slightly stable conditions at night is minimal. Considering this fact and the finding by Lundquist and Chan (2005) that building-induced turbulence is dominant in the urban area, it is justifiable to use the neutral stability assumption in the urban dispersion simulation for IOP 9.

The overall results of this study suggest that the simplified CFD approach implemented in FEM3MP, with explicitly resolved and virtual buildings, can be a cost-effective tool for simulating urban dispersion problems. We will further evaluate and improve our model, with the

goal to produce a sufficiently fast CFD model for integration into the DOE National Atmospheric Release Advisory Center (NARAC) operational modeling system.

Acknowledgments. This work was performed under the auspices of the U.S. Department of Energy by the University of California, Lawrence Livermore National Laboratory under contract No. W-7405-Eng-48. The authors would like to thank Drs. David Stevens, Tom Humphreys and Bob Lee for their contributions to FEM3MP and in the early phase of model evaluation studies using the Joint Urban 2003 data.

References

- Allwine, K., J. Shinn, G. Streit, K. Clawson, and M. Brown, 2002: Overview of URBAN 2000. Bull. Amer. Meteor. Soc., **83**, 521-536.
- Allwine, K., M. Leach, L. Stockham, J. Shinn, R. Hosker, J. Bowers, and J. Pace, 2004: Overview of Joint Urban 2003, AMS Annual Meeting, Seattle, WA, Jan. 11-15, 2004.
- Brown, M. and M. Williams, 1998: An urban canopy parameterization for mesoscale meteorological models. 2nd Sym. on the Urban Environ., Albuquerque, NM, Nov. 1998.
- Brown, M., H. Khalsa, M. Nelson, and D. Boswell, 2004: street canyon flow patterns in a horizontal plane: measurements from the Joint Urban 2003 field experiment. 5th Sym. on the Urban Environ., Vancouver, Canada, Aug. 23-27, 2004.
- Calhoun, R., F. Gouveia, J. Shinn, S. Chan, D. Stevens, R. Lee, and J. Leone, 2004: Flow around a complex building: comparisons between experiments and a Reynolds-averaged Navier-Stokes approach. J. Appl. Meteor., **43**, 696-710.
- _____, F. Gouveia, J. Shinn, S. Chan, D. Stevens, R. Lee, and J. Leone, 2005: Flow around a complex building: experimental and large-eddy simulation comparisons. J. Appl. Meteor., **44**, 571-590.
- Chan, S., D. Ermak, and L. Morris, 1987: FEM3 model simulations of selected Thorny Island Phase I Trials. J. Has. Mat., **16**, 267-292.
- _____, R. Lee, and J. Leone, 1999: FEM3CB modeling of turbulence, aerosols, and UV degradation. Report prepared for Defense Advanced Research Projects Agency. LLNL, Livermore, CA Nov. 1999.

- _____, and D. Stevens, 2000: An evaluation of two advanced turbulence models for simulating the flow and dispersion around buildings. The Millen. NATO/CCMS Int. Tech. Meeting on Air Pollution Modeling and its Application, WIT Press, 355-362.
- _____, D. Stevens, and W. Smith, 2001: Validation of two CFD urban dispersion models using high-resolution wind tunnel data. 3rd Int. Sym. on Environ, Hydraulics, ASU, Tempe, AZ, Dec. 2001, 107.
- _____, R. Lee, and J. Shinn, 2002: Large eddy simulation of turbulent flow and diffusion above and within forest canopies. AMS 12th Joint Conf. on the Application of Air Pollution Meteor. with the Air and Waste Management Assoc., Norfolk, VA, May 2002, 101-102.
- _____, M. Leach, and W. Dannevik, 2003: CFD simulation of a Prairie Grass field dispersion experiment. 7th Annual GMU Transport and Dispersion Modeling Workshop, Fairfax, VA, June 2003.
- _____, T. Humphreys, and R. Lee, 2004: A simplified CFD approach for modeling urban dispersion. AMS Annual Meeting, Seattle, WA, Jan. 11-15, 2004.
- _____, and M. Leach, 2004, Large eddy simulation of an URBAN 2000 experiment with various time-dependent forcing. 5th Sym. on the Urban Environ., Vancouver, Canada, Aug. 23-27, 2004.
- Dyer, A. J., 1974: A review of flux-profile relationships. *Boundary-Layer Meteor.*, **7**, 363-372.
- Gresho, P. and S. Chan, 1998: Projection 2 goes turbulent – and fully implicit. *J. Comp. Fluid Dynamics*, **9**, 249-272.
- Hanna, S., O. Hansen, and S. Dharmavaram, 2005: FLACS CFD air quality model performance evaluation with Kit Fox, Prairie Grass, MUST, and EMU observations. Submitted to *Atmos. Environ.*, 2005.

- Humphreys, T., S. Chan, and R. Lee, 2003: Validation of CFD near building dispersion with URBAN 2000 data for steady and time-dependent boundary conditions. 7th Annual GMU Transport and Dispersion Modeling Workshop, Fairfax, VA, June 2003.
- _____, S. Chan, R. Lee, and E. Peterson, 2004: A validation of simplified CFD approach for modeling urban dispersion with Joint Urban 2003 data. 5th Sym. on the Urban Environ., Vancouver, Canada, Aug. 23-27, 2004.
- Lee, R., and M. Brown, 2001: Building-scale exterior modeling. 2000 DOE CBNP Annual Report, Jan. 2001.
- Lee, R., T. Humphreys, and S. Chan, 2002: High resolution modeling of atmospheric releases around buildings, AMS 12th Joint Conf. on the Application of Air Pollution Meteor. with the Air and Waste Management Assoc., Norfolk, VA, May 2002, j5-6.
- Lundquist, J. K., and S. Chan, 2005: Consequences of urban stability conditions for computational fluid dynamics simulations of urban dispersion. Submitted to J. Appl. Meteor.
- _____, and J. D. Mirocha, 2006: Interaction of nocturnal low-level jets with urban geometries as seen in Joint Urban 2003 data. AMS 6th Sym. on the Urban Environ., Atlanta, GA, Jan 29 – Feb 2, 2006.
- NRC Report of the National Academies, 2003: Tracking and predicting the atmospheric dispersion of hazardous material releases – implications for homeland security. Prepared by the Committee on the Atmospheric Dispersion of Hazardous Material Releases (Chaired by Robert Serafin), 2003.
- Yamada, T., 1982: A numerical model study of turbulent airflow in and above a forest canopy. J. Meteor. Soc., Japan, **60**, 439-454.

Zeierman, S., and M. Wolfshtein, 1986: Turbulent time scale for turbulent-flow calculations.

AIAA Journal, **24**, 1606-1610.

List of Captions

- Fig. 1. Predicted velocity and concentration on the vertical plane of symmetry with the cube modeled as a virtual building (top three panels) and as a solid building (bottom panel). The values of drag coefficient used in the virtual building approach are 15, 50, and 100, respectively.
- Fig. 2. Predicted velocity and concentration on the plane $z/H = 0.2$ with the cube modeled as a virtual building (top three panels) and as a solid building (bottom panel). The values of drag coefficient used in the virtual building approach are 15, 50, and 100, respectively.
- Fig. 3. Footprints of buildings in the central business district of OKC and release points: S3 (at botanical gardens) for IOP 3 and S9 (on Park Ave) for IOP 9.
- Fig. 4. Comparison of inflow wind speed and direction profiles (solid lines) against sodar data (dashed lines) for (a) IOP 3 with sodar located near the botanical gardens, and (b) IOP 9 with sodar located at ~ 4 km downwind of OKC.
- Fig. 5. Predicted wind vectors and wind speeds (gray scale contours) on $z=2$ m plane for IOP3, illustrating the complexity of airflow near buildings.
- Fig. 6. Comparison of predicted wind vectors (without arrow heads) against 30-min averaged data (with arrow heads) measured by DPG PWIDS and sonic anemometers (in Park Avenue, $y=430$ to 460 m) on $z=8$ m plane for IOP 3.
- Fig. 7. Comparison of predicted versus observed profiles of four variables at the crane station for IOP 3: wind speed (upper left), wind direction (upper right), friction velocity (lower left), and TKE (lower right).

Fig. 8. Comparison of predicted versus observed concentrations along Broadway Avenue for IOP

3. Solid line - predictions with NEV and neutral stability, dashed line - predictions with LEV and unstable effects, circles - observed data.

Fig. 9. Comparison of predicted concentration patterns versus measured data (small squares with the same color scheme) in the source area of IOP 3.

Fig. 10. Predicted wind vectors and wind speeds (gray scale contours) on $z=2$ m plane for IOP 9, illustrating the complexity of airflow in the source area.

Fig. 11. Comparison of predicted wind vectors (without arrow heads) against 30-min average data (with arrow heads) measured by DPG PWIDS and sonic anemometers (in Park Avenue, $y=430$ to 460 m) on $z=8$ m plane for IOP 9.

Fig. 12. Comparison of predicted versus observed profiles of four variables at the crane station for IOP 9: wind speed (upper left), wind direction (upper right), friction velocity (lower left), and TKE (lower right).

Fig. 13. Comparison of predicted versus observed concentrations along plume 'centerline' for IOP 9. Solid line - predictions with NEV and neutral stability, dashed line - predictions with LEV and stable effects, circles - observed data. The peak value of concentration predicted by the NEV turbulence model is 10,272 ppb near the source.

Fig. 14. Comparison of predicted concentration patterns versus measured data (small squares with the same color scheme) in the source area of IOP 9.

Fig. 15. Vertical structure of the plume of IOP 9:

(a) Predicted (blue lines) versus observed (green lines) concentration profiles around building (B1) at the northeast corner of Park Avenue in Fig. 14, and

- (b) Velocity vectors and concentration patterns on a vertical plane to illustrate lofting of the plume caused by updrafts in building wakes.

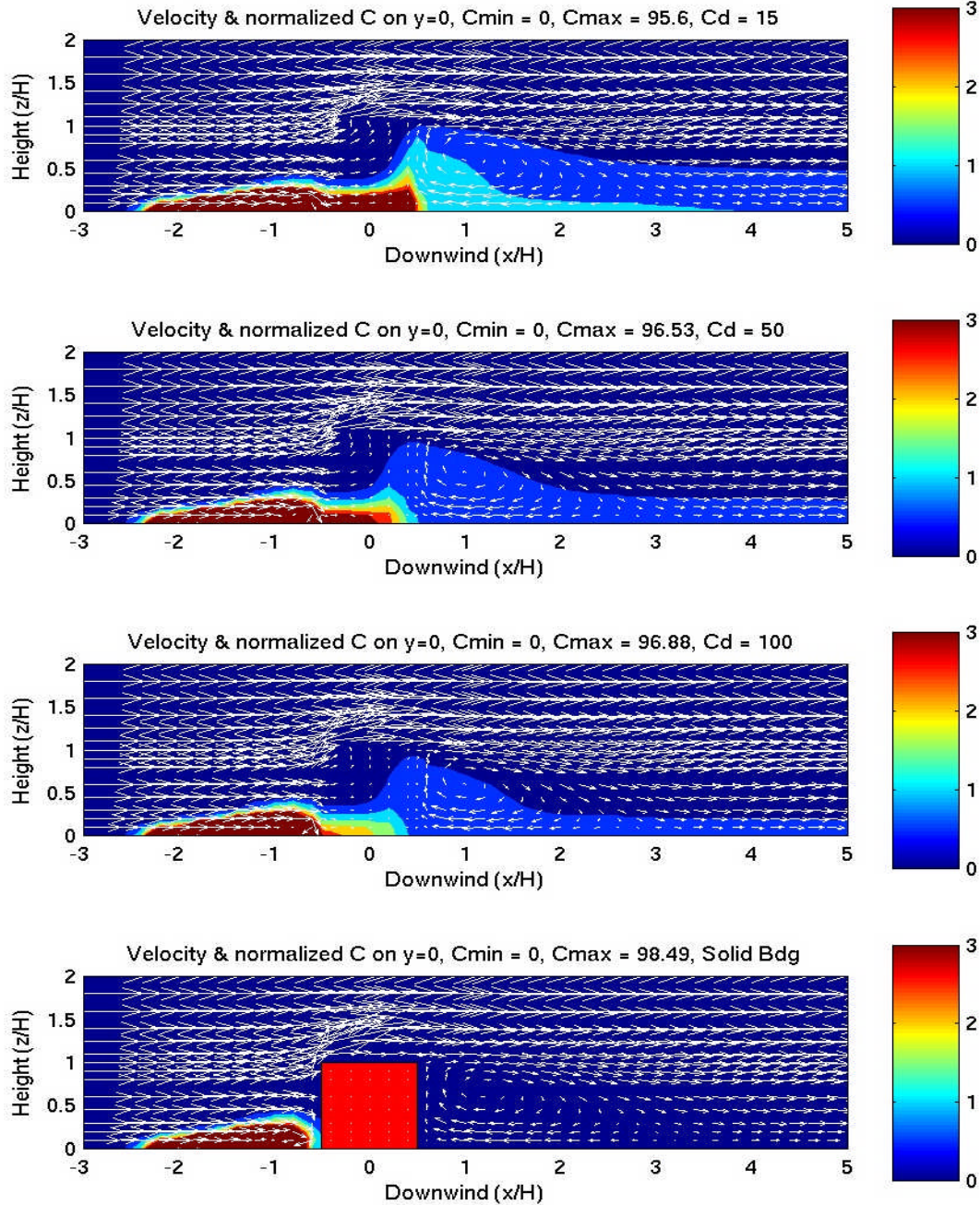


Fig. 1. Predicted velocity and concentration on the vertical plane of symmetry with the cube modeled as a virtual building (top three panels) and as a solid building (bottom panel). The values of drag coefficient used in the virtual building approach are 15, 50, and 100, respectively.

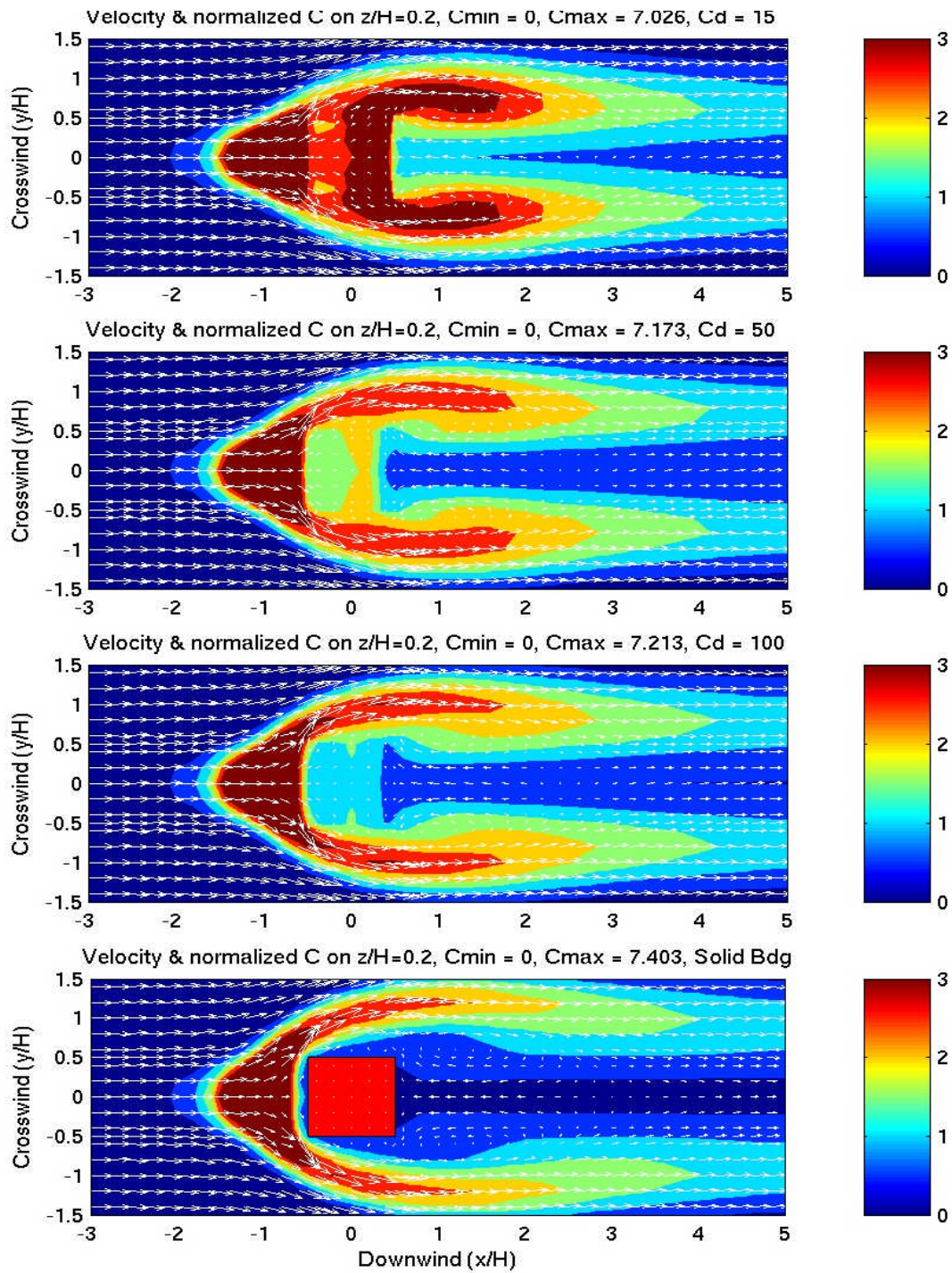


Fig. 2. Predicted velocity and concentration on the plane $z/H = 0.2$ with the cube modeled as a virtual building (top three panels) and as a solid building (bottom panel). The values of drag coefficient used in the virtual building approach are 15, 50, and 100, respectively.

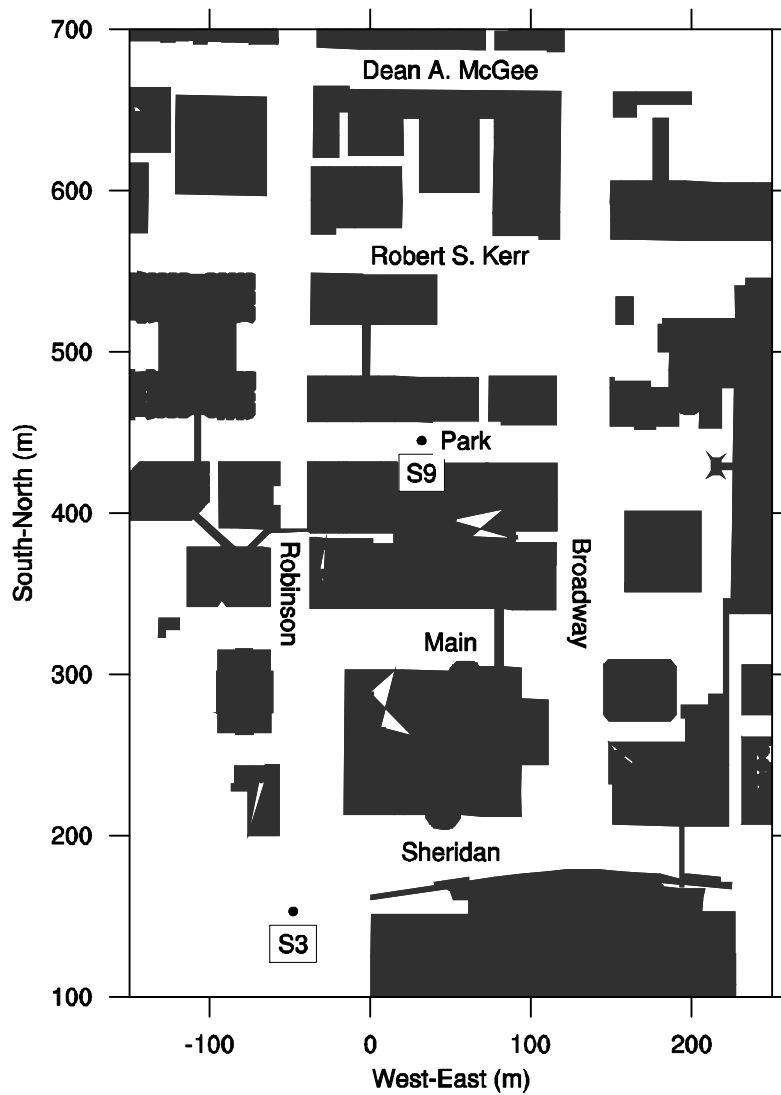
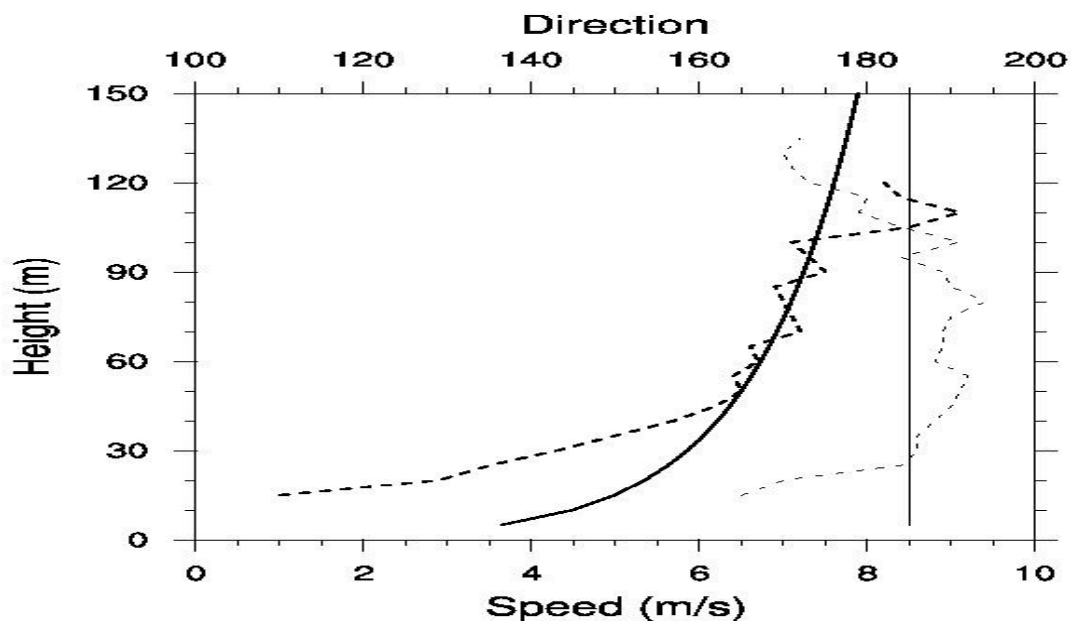


Fig. 3. Footprints of buildings in the central business district of OKC and release points: S3 (at botanical gardens) for IOP 3 and S9 (on Park Ave) for IOP 9.

(a) IOP 3



(b) IOP 9

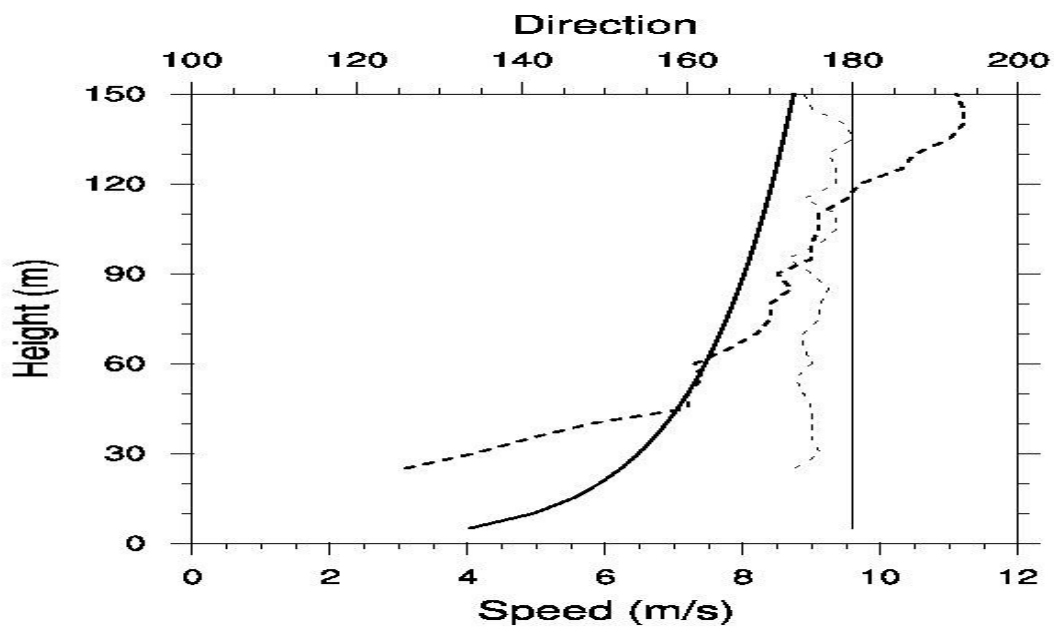


Fig. 4. Comparison of inflow wind speed and direction profiles (solid lines) against sodar data (dashed lines) for (a) IOP 3 with sodar located near the botanical gardens, and (b) IOP 9 with sodar located at ~ 4 km downwind of OKC.

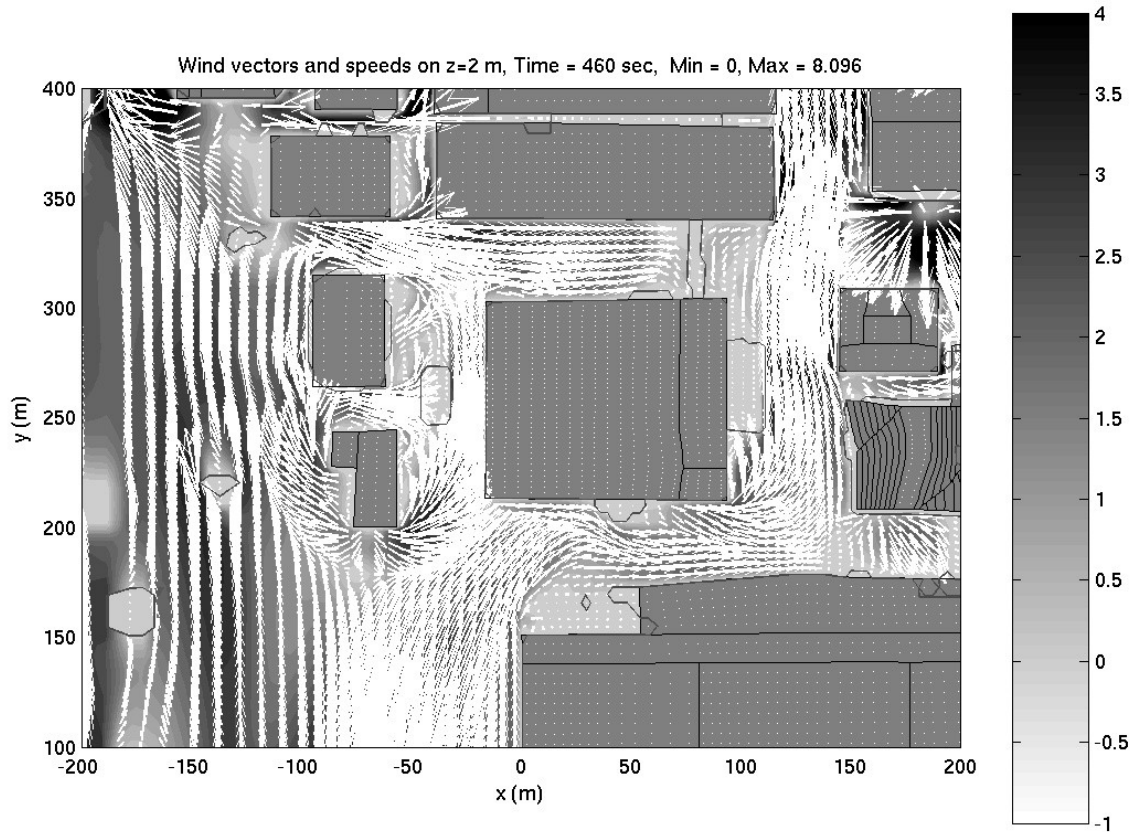


Fig. 5. Predicted wind vectors and wind speeds (gray scale contours) on $z=2$ m plane for IOP3, illustrating the complexity of airflow near buildings.

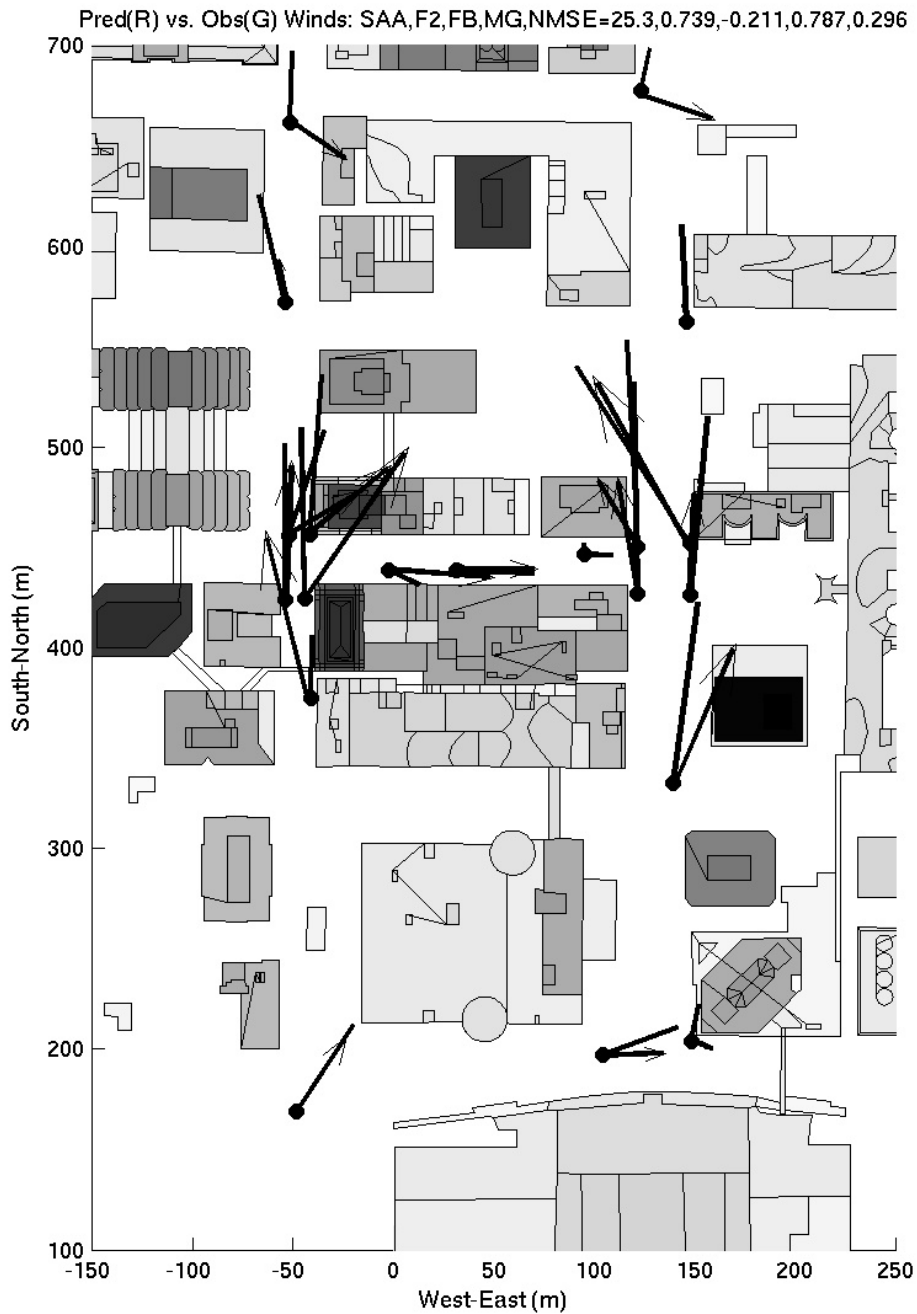


Fig. 6. Comparison of predicted wind vectors (without arrow heads) against 30-min averaged data (with arrow heads) measured by DPG PWIDS and sonic anemometers (in Park Avenue, $y=430$ to 460 m) on $z=8$ m plane for IOP 3.

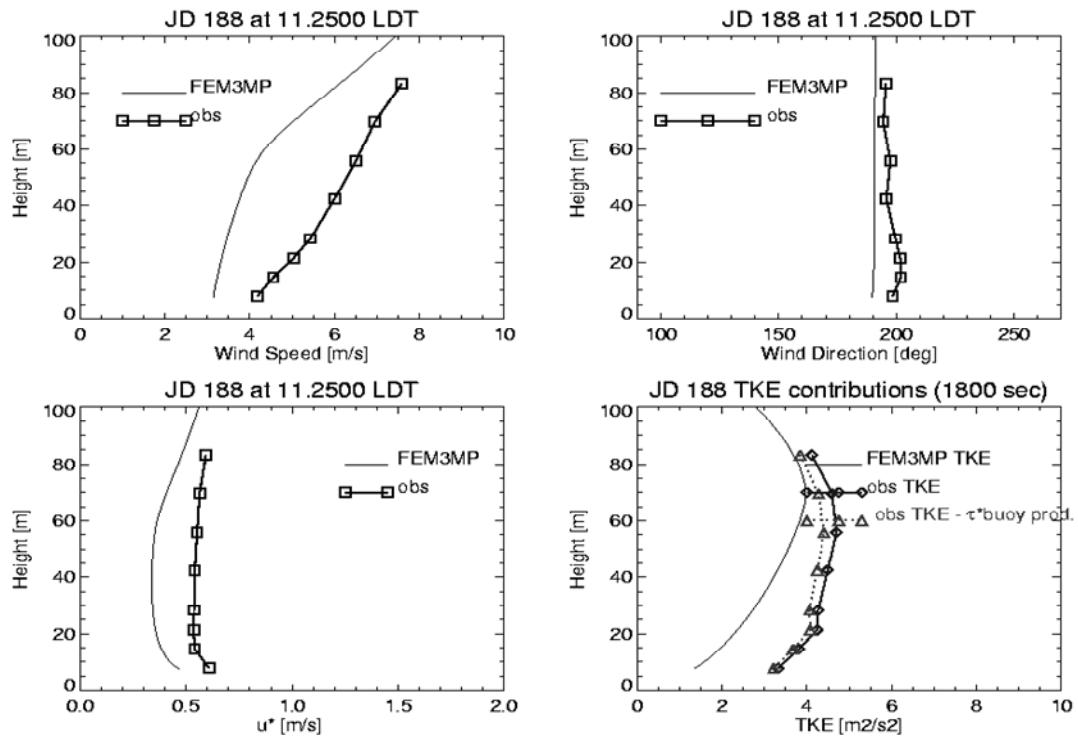


Fig. 7. Comparison of predicted versus observed profiles of four variables at the crane station for IOP 3: wind speed (upper left), wind direction (upper right), friction velocity (lower left), and TKE (lower right).

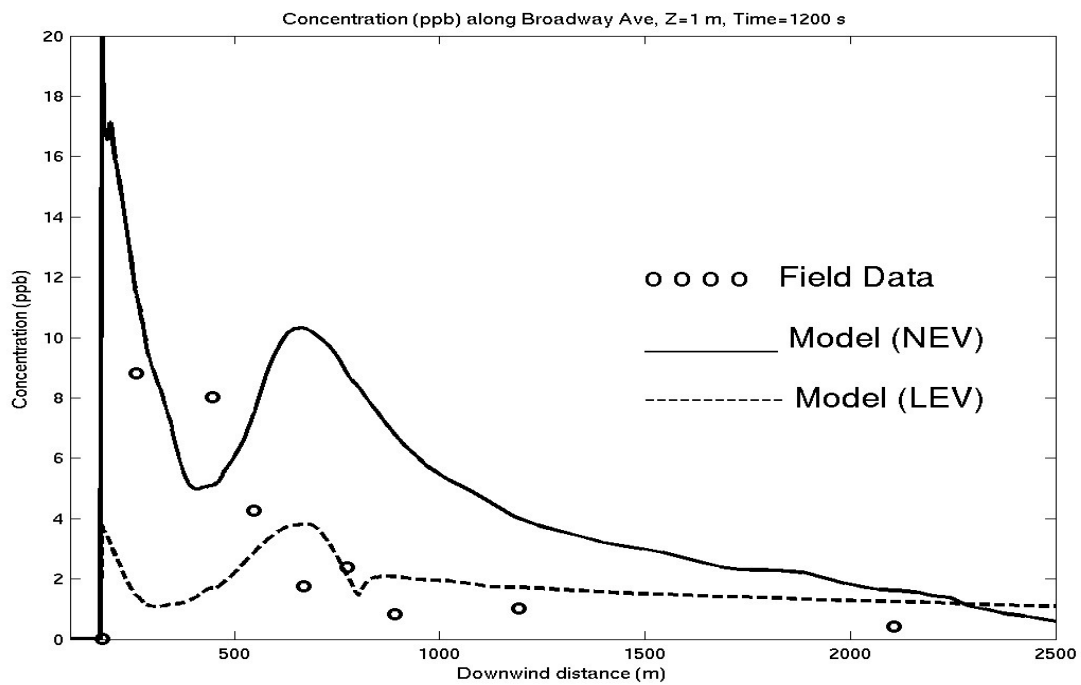


Fig. 8. Comparison of predicted versus observed concentrations along Broadway Avenue for IOP

3. Solid line - predictions with NEV and neutral stability, dashed line - predictions with LEV and unstable effects, circles - observed data.

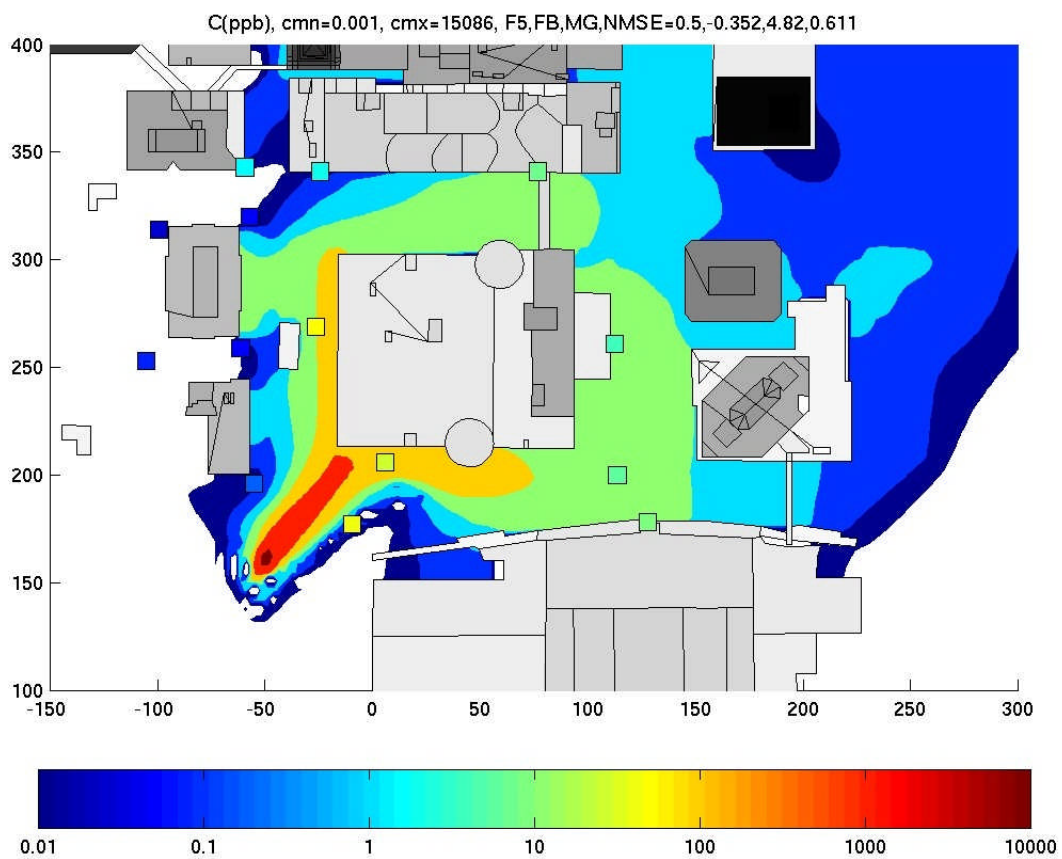


Fig. 9. Comparison of predicted concentration patterns versus measured data (small squares with the same color scheme) in the source area of IOP 3.

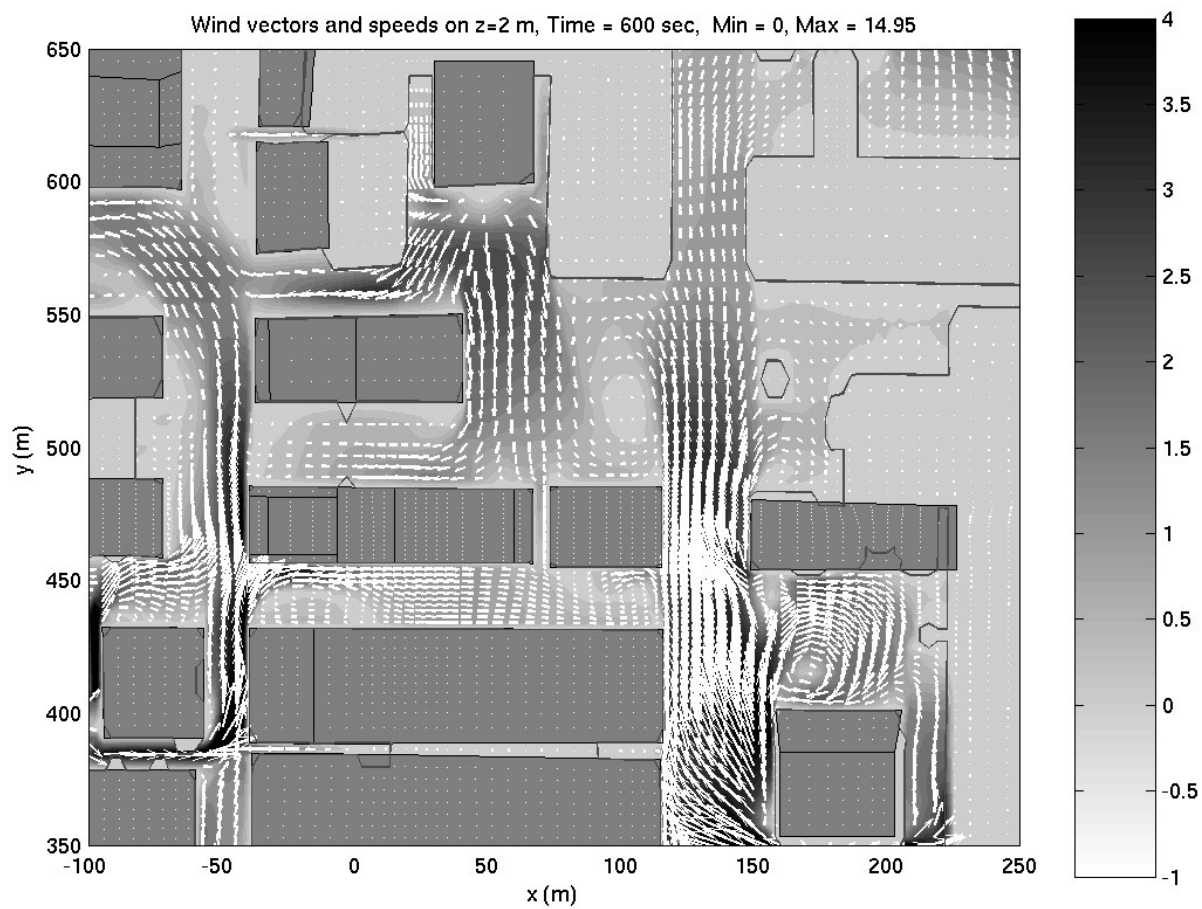


Fig. 10. Predicted wind vectors and wind speeds (gray scale contours) on $z=2$ m plane for IOP 9, illustrating the complexity of airflow in the source area.

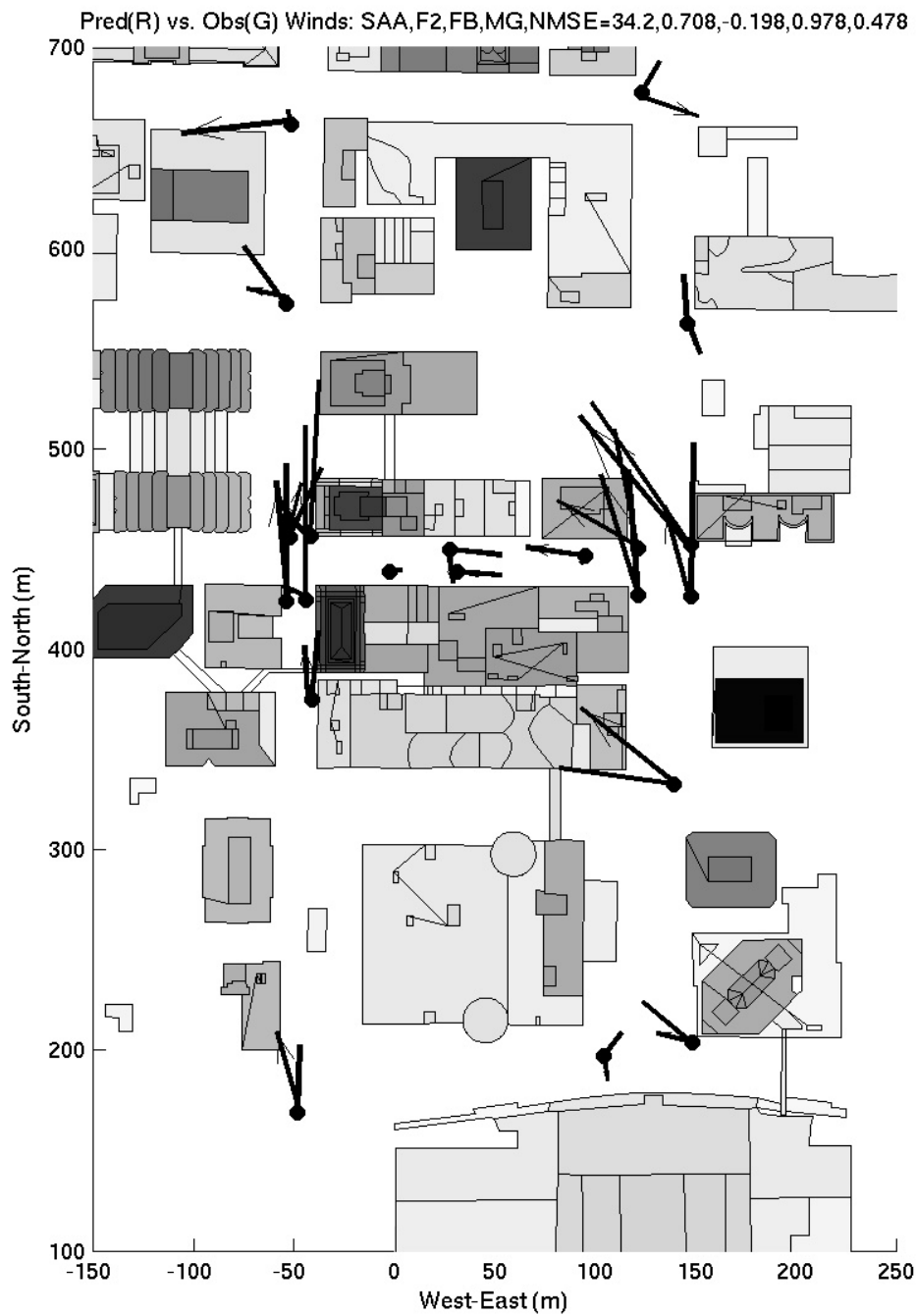


Fig. 11. Comparison of predicted wind vectors (without arrow heads) against 30-min average data (with arrow heads) measured by DPG PWIDS and sonic anemometers (in Park Avenue, $y=430$ to 460 m) on $z=8$ m plane for IOP 9.

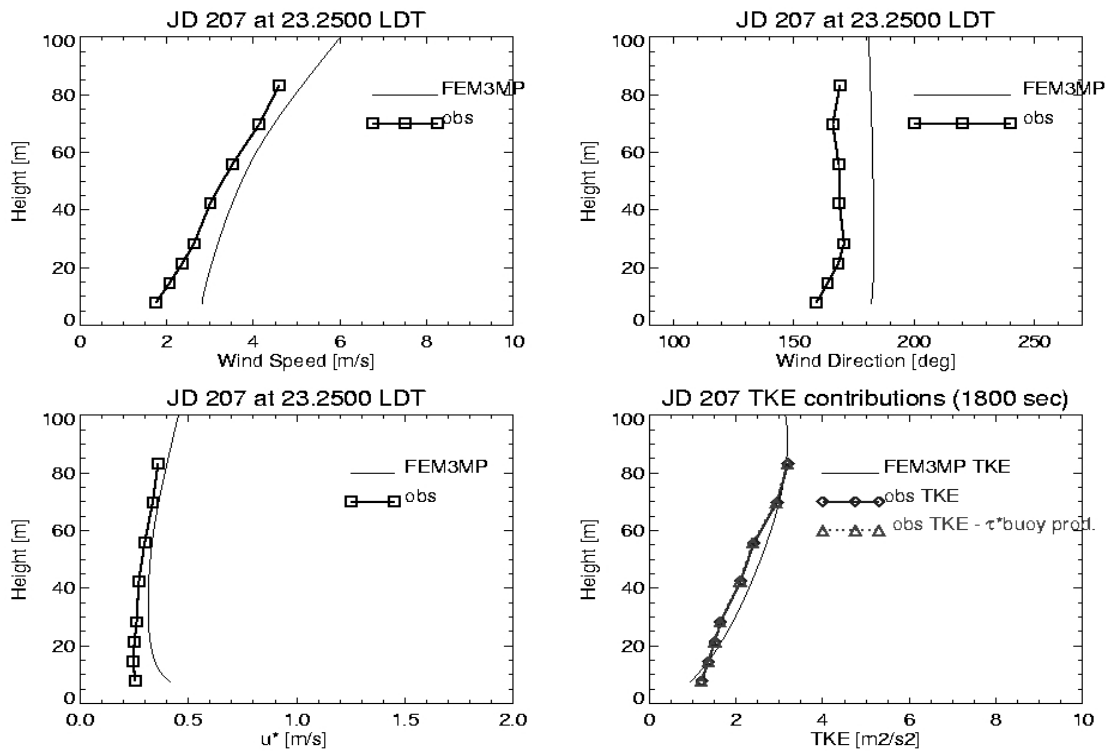


Fig. 12. Comparison of predicted versus observed profiles of four variables at the crane station for IOP 9: wind speed (upper left), wind direction (upper right), friction velocity (lower left), and TKE (lower right).

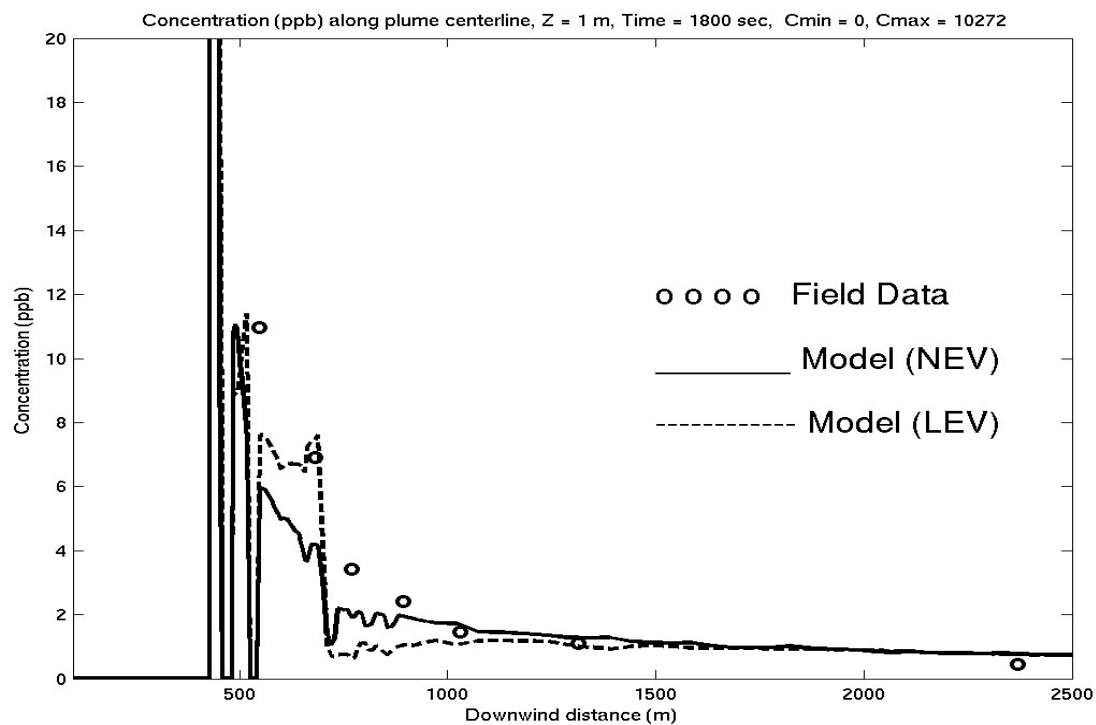


Fig. 13. Comparison of predicted versus observed concentrations along plume 'centerline' for IOP 9. Solid line - predictions with NEV and neutral stability, dashed line - predictions with LEV and stable effects, circles - observed data. The peak value of concentration predicted by the NEV turbulence model is 10,272 ppb near the source.

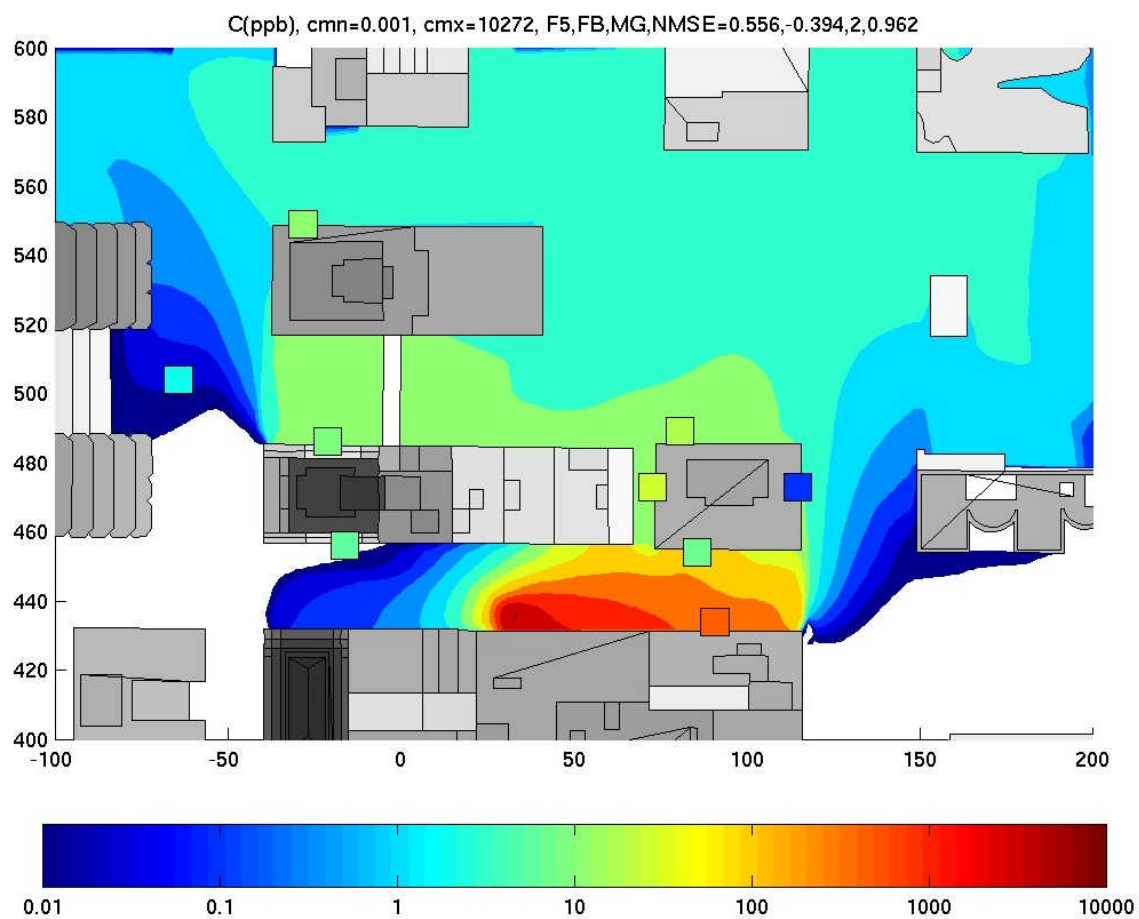
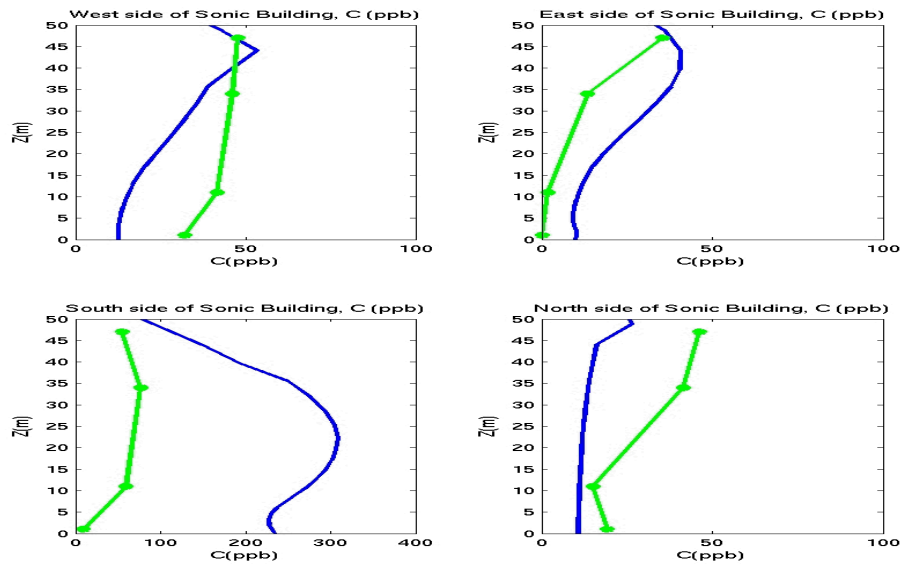


Fig. 14. Comparison of predicted concentration patterns versus measured data (small squares with the same color scheme) in the source area of IOP 9.

(a) Predicted vs. observed concentration profiles



(b) Velocity and concentration on a vertical plane

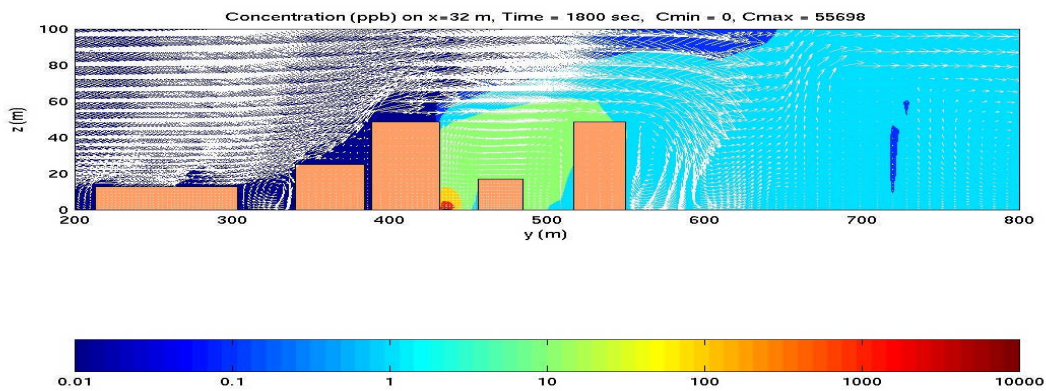


Fig. 15. Vertical structure of the plume of IOP 9:

- (a) Predicted (blue lines) versus observed (green lines) concentration profiles around building (B1) at the northeast corner of Park Avenue in Fig. 14, and
- (b) Velocity vectors and concentration patterns on a vertical plane to illustrate lofting of the plume caused by updrafts in building wakes.